



Real-time atomic deformation behavior of nano CoCrCuFeNi high-entropy alloy

Yong-gang TONG¹, Nan TIAN¹, Hao CHEN², Xian-cheng ZHANG²,
Yong-le HU¹, Xi-xi JI¹, Ming-jun ZHANG¹, Chao-jie ZHAO¹

1. College of Automobile and Mechanical Engineering,
Changsha University of Science and Technology, Changsha 410114, China;
2. College of Mechanical and Power Engineering,
East China University of Science and Technology, Shanghai 200237, China

Received 11 November 2021; accepted 25 February 2022

Abstract: Tensile tests were performed by molecular dynamics at various strain rates ranging from 2×10^8 to $1 \times 10^{10} \text{ s}^{-1}$ and various temperatures ranging from 10 to 1200 K, and the real-time deformation behavior of a nanocrystalline CoCrCuFeNi high-entropy alloy was investigated. The results indicate that the main deformation mechanism is grain boundary slip at high temperatures and low strain rates. Dislocation slip replaces grain boundary slip to control plastic deformation with decreasing temperature and increasing strain rate, correspondingly enhancing the strength of the alloy. Furthermore, the alloys with different grain sizes were simulated to evaluate the effects of grain boundaries on the mechanical behavior. It is found that the strength of the nanocrystalline high-entropy alloys increases with increasing grain sizes when the grain size is too small, exhibiting an inverse Hall–Petch relationship.

Key words: nanocrystalline high-entropy alloy; dislocation evolution; deformation mechanism; strain rate; grain size

1 Introduction

Unlike conventional alloys that contain only one or two primary elements, high-entropy alloys (HEAs) are a new type of alloys that contain four or more primary elements, which have attracted extensive attention for their potential applicability in engineering [1]. The multi-principal characteristic makes them exhibit the synergy of multiple mechanisms (including dislocation mechanism, deformation twinning, phase transformation, etc.) during the deformation process, resulting in excellent mechanical properties, such as high hardness and strength, good ductility, excellent thermal stability and corrosion resistance at ultra-high temperatures [2–8].

Due to the multicomponents and complex structure of HEAs, the tunability is greatly enhanced. Numerous toughening strategies have been proposed to achieve even simultaneous increases in strength and toughness [9]. As an effective means of toughening, grain refinement has been extensively investigated experimentally. For example, LIU et al [10] investigated the grain growth mechanism of CoCrFeNiMn HEAs at different annealing temperatures and found that the relationship between hardness and grain size followed the classical Hall–Petch equation. SEOL et al [11] doped FeCoCrNiMn and Fe₄₀Mn₄₀Cr₁₀-Co₁₀ HEAs with B elements to control the grain growth to achieve refinement. However, the grain size of the alloy cannot be precisely controlled by experimental studies and the changes in crystal

Corresponding author: Yong-gang TONG, E-mail: tongyonggang_csust@163.com;
Xian-cheng ZHANG, E-mail: xczhang@ecust.edu.cn

DOI: 10.1016/S1003-6326(23)66172-2

1003-6326/© 2023 The Nonferrous Metals Society of China. Published by Elsevier Ltd & Science Press

structure and grain boundaries (GB) cannot be observed at the atomic scale in real time. As a powerful complement of experiment, molecular dynamics (MD) simulation can provide a continuous and intuitive microscopic evolution to elucidate the deformation mechanism at the atomic scale of HEA. For instance, JIANG et al [12] investigated the effect of Al content on the microstructural evolution and mechanical properties of $\text{Al}_x\text{CoCrFeNi}$. CAO et al [13] investigated the plastic deformation mechanism of CoCrNi by MD simulation and found that it is related to local chemical inhomogeneity. Unfortunately, MD studies on the effect of grain size on the mechanical properties and deformation behavior of HEA are rarely involved. Therefore, nanocrystalline HEAs with different grain sizes were constructed to investigate the effect of GBs during deformation. In addition, considering the application of nanocrystalline HEA in practical environments, we investigated the deformation behavior of nanocrystalline CoCrCuFeNi HEA at different temperatures and strain rates from the atomic scale by MD simulations. Understanding the deformation mechanism of nanocrystalline HEAs provides further insights for the design of strengthening and toughening HEA.

2 Simulation methods

In order to obtain the polycrystalline HEA model, ten randomly-oriented grains were constructed by Voronoi construction method [14,15], as shown in Figs. 1(a, b). The size of the model is $20\text{ nm} \times 20\text{ nm} \times 20\text{ nm}$ and the model contains more than 710000 atoms. Five types of atoms (Co, Cr, Cu, Fe and Ni) were randomly distributed in the FCC lattice. MD simulations were realized by using the LAMMPS [16]. The atomic interactions were described using the embedded atom method (EAM) developed by FARKAS and CARO [17]. Periodic boundary conditions were employed in all directions. All samples were energy minimized by using a conjugate gradient algorithm and relaxed for 100 ps under the isothermal–isobaric ensemble (NPT). The time step of the simulation was 1 fs. After the equilibration process, tensile loads were applied along the x -axis at different temperatures (10, 300, 800, and 1200 K) and strain rates (2×10^8 , 1×10^9 , 5×10^9 , 8×10^9 and $1 \times 10^{10}\text{ s}^{-1}$) to a final strain

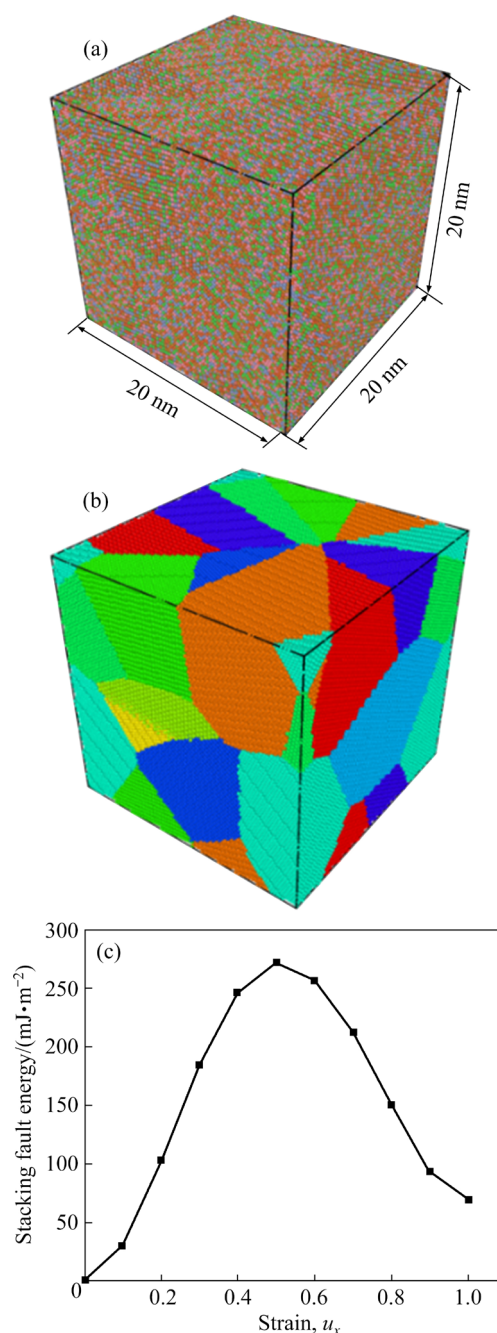


Fig. 1 CoCrCuFeNi HEA model of FCC phase simulated by MD: (a) Model colored according to atomic types; (b) Model colored according to grain types; (c) Strain–stacking fault energy curve

of 12%, respectively. Ovito software was used for visualization to track atomic motion in real time [18]. Common-neighbor analysis (CNA) was used to distinguish atomic structure [19]. Motion of dislocations was tracked by dislocation extraction algorithm (DXA) [20]. Many stacking faults and twins are produced during the deformation of nanocrystals, which is related to its stacking fault energy (SFE). Therefore, we slipped the crystal on

the {111} slip surface along the $\langle 112 \rangle$ direction to simulate the stacking fault, which results in a calculated SFE of 69.16 mJ/m² for CoCrCuFeNi HEA, as shown in Fig. 1(c). This simulation result is consistent with the value of 67.445 mJ/m² obtained by LIU [21].

3 Results and discussion

3.1 Mechanical performance

The stress–strain relationships of CoCrCuFeNi HEA at different temperatures and strain rates are shown in Fig. 2. Due to the softening effect at high temperature, the tensile strength of HEA decreases with increasing temperature. The effect of strain rate on tensile strength is also obvious. Due to the short duration, the strain rates of the MD simulations are all high, much higher than the experimental tensile rates. The results of the MD simulations are definitely more complex compared with the experimental ones because the high strain rates lead to more complex deformation mechanisms, such as the generation of more

deformation twins relative to the low strain rate deformation [22]. As shown in Fig. 2, the tensile strength and elasticity modulus increase significantly with increasing strain rate. At lower strain rates, the stress fluctuation during plastic deformation is significant, which is related to the inhomogeneity of stress distribution. Figure 3 shows the relationship between average flow stress, ultimate strength and strain and the corresponding fitting curves. The calculated result is consistent with the conclusion of LI et al [23], that is, it satisfies the power function $\sigma = a + b\dot{\epsilon}^c$, where σ and $\dot{\epsilon}$ represent average flow stress and strain rate respectively, and a , b , and c represent the fitting parameters. The fitting parameters obtained under different stretching conditions are given in Tables 1 and 2. It can be seen that the effect of temperature on each fitting parameter is very obvious. The average flow stress and ultimate strength (i.e., parameter a) under quasi-static conditions ($\dot{\epsilon} = 0$) can be obtained from the power function. Therefore, the ultimate strength of HEA at 300 K is obtained as 3.80 GPa, which is higher than the experimental

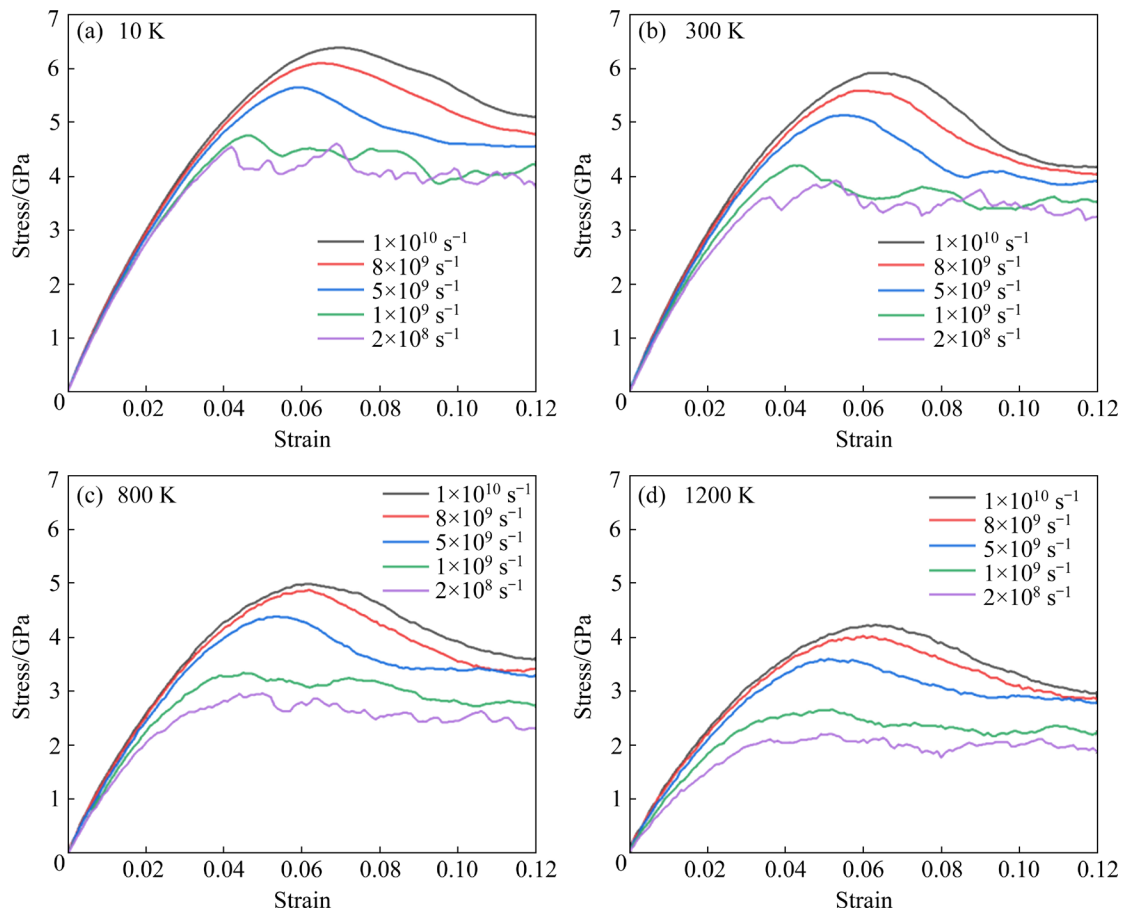


Fig. 2 Stress–strain curves at different temperatures (10, 300, 800, and 1200 K) and strain rates (2×10^8 , 1×10^9 , 5×10^9 , 8×10^9 and $1 \times 10^{10} \text{ s}^{-1}$) in CoCrCuFeNi HEA

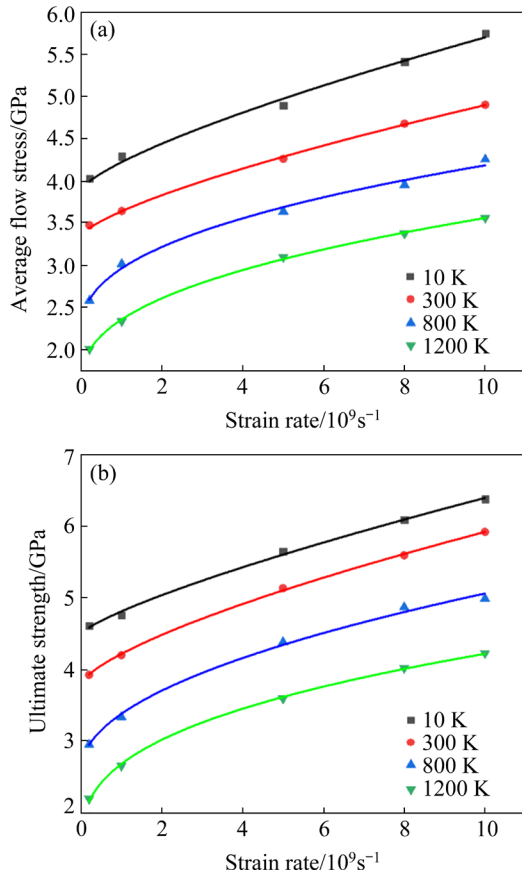


Fig. 3 Variation of average flow stress (a) and ultimate strength (b) with strain rate at different temperatures and corresponding fitting curves

Table 1 Fitting parameters of ultimate strengths at different temperatures

Temperature/K	<i>a</i>	<i>b</i>	<i>c</i>
10	~4.50	3.120×10^{-8}	0.7785
300	~3.80	2.111×10^{-7}	0.7003
800	~2.60	2.713×10^{-5}	0.4958
1200	~1.50	6.707×10^{-4}	0.3609

Table 2 Fitting parameters of average flow stresses at different temperatures

Temperature/K	<i>a</i>	<i>b</i>	<i>c</i>
10	~3.90	6.627×10^{-8}	0.7436
300	~3.35	8.740×10^{-8}	0.725
800	~2.20	1.406×10^{-4}	0.415
1200	~1.60	1.453×10^{-4}	0.413

value obtained by KIM et al [24]. The reason for this fact may be that the calculated model is a more idealized single-phase polycrystalline model, while the experimentally prepared as-cast CoCrFeCuNi

HEA contains impurities and a large number of defects.

3.2 Deformation behavior

To reveal the effects of temperature and strain rate on the deformation mechanism, the structural distribution and dislocation evolution of nanocrystalline HEAs after tensile deformation were investigated. Figure 4 shows the distribution of dislocations and structures of nanocrystalline HEA at different temperatures and strain rates at 12% strain. In Figs. 4(a–d), green, blue and red represent FCC, BCC and HCP structures, respectively, and white represents disordered atoms and GBs. In Figs. 4(e–f), blue line represents complete dislocations, green line represents Shockley dislocations, yellow line represents Hirth dislocations, pink line represents stair-rod dislocations, light blue line represents Frank dislocations, and red line represents other dislocations. It can be found that the plastic deformation is mainly controlled by dislocation slip and GB slip. Dislocation occurs with the density from high to low under the conditions of: 10 K and $1 \times 10^{10} \text{ s}^{-1}$ ($30.24 \times 10^{16} \text{ m}^{-2}$), 10 K and $2 \times 10^8 \text{ s}^{-1}$ ($23.35 \times 10^{16} \text{ m}^{-2}$), 1200 K and $1 \times 10^{10} \text{ s}^{-1}$ ($19.94 \times 10^{16} \text{ m}^{-2}$), and 1200 K and $2 \times 10^8 \text{ s}^{-1}$ ($15.49 \times 10^{16} \text{ m}^{-2}$). At low strain rates, most of the dislocations are mainly distributed near the GBs and then slide parallel to them, as shown in Figs. 4(a, c). And at high strain rates, these dislocations are no longer parallel to each other, but interact and entangle with each other, as shown in Figs. 4(b, d). By comparing Figs. 4(e) and 4(f) (or Figs. 4(g) and 4(h)), it can be found that the dislocation density is higher at high strain rates, so that the ultimate strength of the material increases with the increase of strain rate. The microstructure and dislocation evolution of the samples at low temperatures are shown in Figs. 4(a, b, e, f). It can be found that a large number of dislocations generate at low temperature and cluster near the GBs. The microstructure and dislocation evolution of the samples at high temperatures are shown in Figs. 4(c, d, g, h). The disordered atoms at the GBs diffuse and the GBs slip significantly at high temperatures. By comparing Figs. 4(e) and 4(g) (or Figs. 4(f) and 4(h)), it can be found that the dislocation density at high temperature is significantly lower than that at low temperature. The energy barrier of GB slip

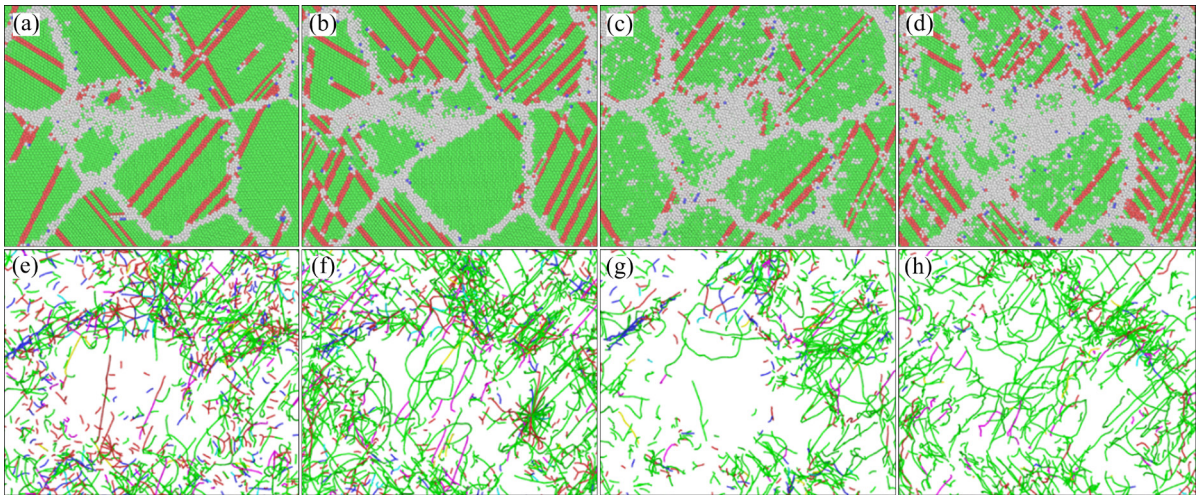


Fig. 4 Structure distribution (a–d) and dislocation distribution (e–h) after tensile deformation under different conditions: (a, e) 10 K and $2 \times 10^8 \text{ s}^{-1}$; (b, f) 10 K and $1 \times 10^{10} \text{ s}^{-1}$; (c, g) 1200 K and $2 \times 10^8 \text{ s}^{-1}$; (d, h) 1200 K and $1 \times 10^{10} \text{ s}^{-1}$

decreases more rapidly compared to dislocation nucleation, leading to a deformation mechanism dominated by GB slip at high temperatures [25,26].

3.3 Effect of grain sizes

According to the classical Hall–Petch relationship, the smaller the grain size, the higher the strength of the material [27–30]. Therefore, grain refinement as a strengthening means is used to improve the mechanical properties of materials. In order to investigate the effect of GBs on the mechanical properties and deformation behavior of HEAs, the tensile tests of nanocrystalline CoCuFeNi HEAs with different grain sizes ($d=7.94, 6.28, 5.47, 4.98, 4.51, 3.61, 3.16, 2.88$ and 2.67 nm) were carried out. The results show that the ultimate strength increases with increasing grain size for a certain range of grain sizes, showing an inverse Hall–Petch relationship [31–33], i.e., the smaller the grain size, the lower the strength, as shown in Fig. 5(a). The equation obtained by fitting is $\sigma_s=9.06-8.19d^{-1/2}$, where σ_s represents the yield strength and d represents the average grain size. This is consistent with the results obtained experimentally by HU et al [34], where the Hall–Petch law fails and the grain is softened when the grain size is below 10 nm.

In order to understand the effect of grain sizes on the mechanical performance and deformation behavior, the atomic structure and dislocation motion of nanocrystalline HEA with different grain sizes were studied. With the continuous loading of tensile stress, when the dislocation moves to the GB

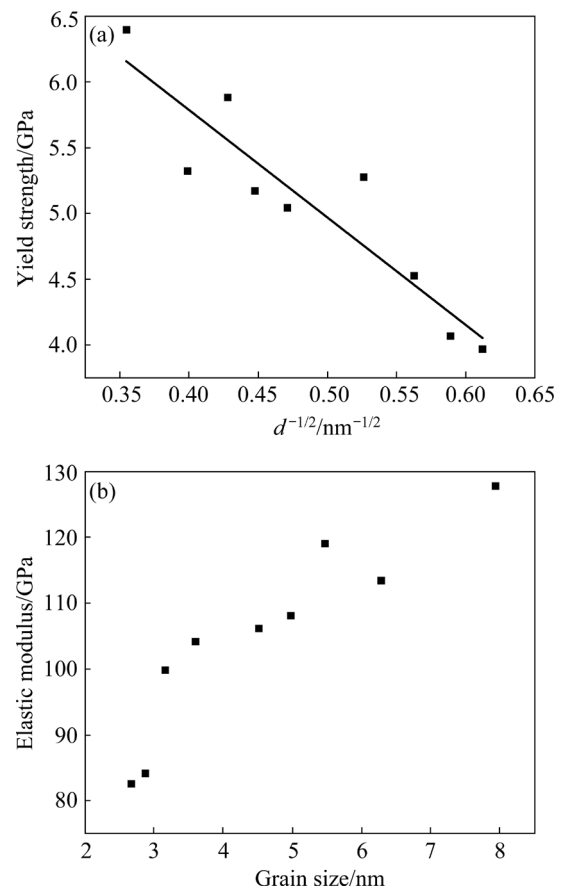


Fig. 5 Variation of yield strength (a) and elastic modulus (b) with grain size

position, the dislocation cannot be transferred to the next grain due to the different crystal orientations of the grains on both sides of the GB. Dislocations continue to accumulate at the GBs (Figs. 6(a–c)), resulting in higher stress concentrations at the GBs.

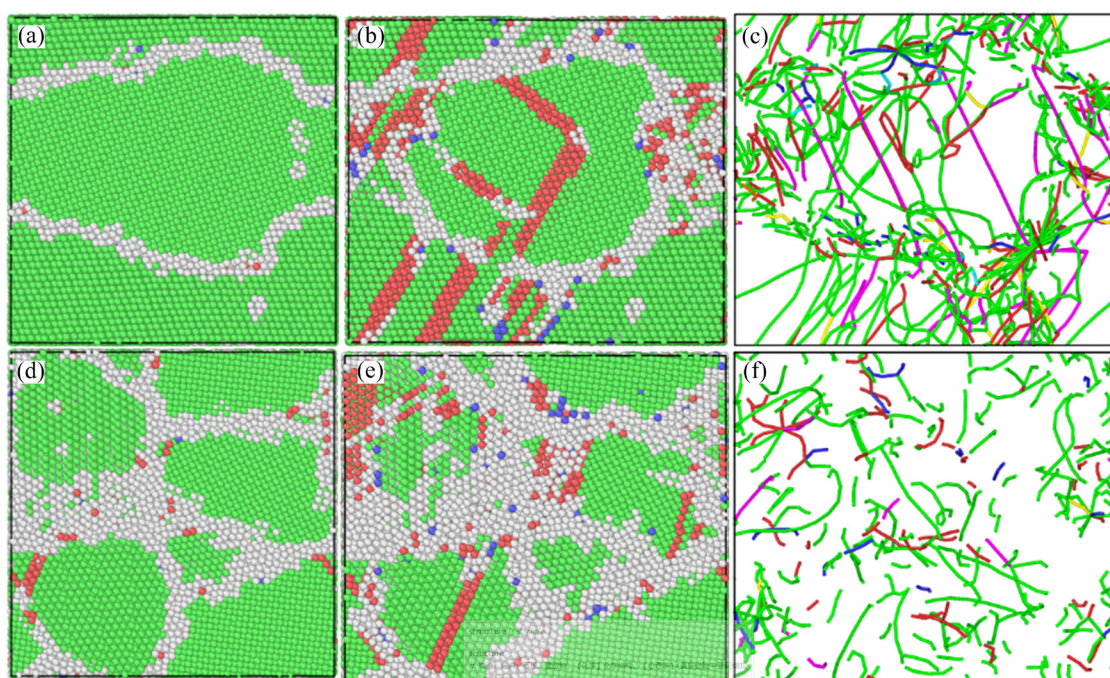


Fig. 6 Initial structure (a), final structure (b) and dislocations (c) at 12% deformation with $d=7.94$ nm; Initial structure (d), final structure (e) and dislocations (f) at 12% deformation with $d=4.51$ nm

The stress accumulated to a certain extent becomes the driving force for the dislocation sources at the adjacent GBs, and finally leads to the dislocation movement. When the grain size is too small, the number of atoms contained in every grain is very small. At this time, the movement of dislocations inside the grain is difficult to proceed, and the phenomenon of dislocation pile-up does not occur at the GB (Fig. 6(f)). In the nanocrystalline model, the hindering effect of GBs on dislocation in the grains is very small and can be ignored due to the small grain size. GB slip becomes the main deformation mechanism. When the grain size continues to decrease, the volume fraction of GB increases (Figs. 6(d, e)), and the GB stability becomes worse. GB slip is easier to proceed, which inevitably leads to a decrease in strength.

Figure 5(b) shows the variation of elastic modulus with average grain size. It can be seen that the elastic modulus decreases with the decrease of the average grain size. This result is in agreement with that obtained from experiments by CHEN [35]. It is concluded that the elastic modulus is related to the volume fraction of GB. Due to the inherent structure of GB, the volume fraction of GB increases with the decrease of grain size. As shown in Figs. 6(a, d), the smaller the grain size, the more

disordered state the atoms at the GBs, and the larger the volume fraction of the GB. Therefore, too small grain size leads to grain boundary instability, which weakens the ability of the material to resist elastic deformation.

4 Conclusions

(1) The ultimate strength and average flow stress of HEA decrease with increasing temperature. The plastic deformation mechanism at low temperatures is dominated by dislocation slip, while GB slip dominates at high temperatures.

(2) Higher strain rates lead to higher ultimate strengths and average flow stresses. At low strain rates, dislocations are mainly distributed near GBs and then slide parallel to them, while at high strain rates, dislocations interact with each other and become entangled.

(3) For nanocrystalline HEA, the larger the grain size, the higher the strength, showing the inverse Hall–Petch law. When the size is too small, the number of atoms contained in each grain is so small that dislocation movement within the grain is difficult and does not produce dislocation blockage at GBs, which leads to a decrease in strength with decreasing size.

Acknowledgments

This work was supported by National Natural Science Foundation of China (Nos. 92166105, 52005053, 5180052032), High-Tech Industry Science and Technology Innovation Leading Program of Hunan Province, China (No. 2020GK2085), Hunan Youth Science and Technology Innovation Talent Project, China (No. 2021RC3096), and Open Fund of Key Laboratory of New Processing Technology for Nonferrous Metal & Materials Ministry of Education, China (No. 20KF-24).

References

- [1] DU Xin, LU Xiao-chong, SHUANG Si-yao, WANG Zhang-wei, XIONG Qi-lin, KANG Guo-zheng, ZHANG Xu. Cyclic plasticity of CoCrFeMnNi high-entropy alloy (HEA): A molecular dynamics simulation [J]. *International Journal of Applied Mechanics*, 2021, 13: 2150006.
- [2] BAHADUR F, BISWAS K, GURAO N P. Micro-mechanisms of microstructural damage due to low cycle fatigue in CoCuFeMnNi high entropy alloy [J]. *International Journal of Fatigue*, 2020, 130: 105258.
- [3] KLIMOVA M V, SEMENYUK A O, SHAYSULTANOV D G, SALISHCHEV G A, STEPANOV N D. Effect of carbon on cryogenic tensile behavior of CoCrFeMnNi-type high entropy alloys [J]. *Journal of Alloys and Compounds*, 2019, 811: 152000.
- [4] LI Yan-gen, LI Rui-li, PENG Qing. Enhanced surface bombardment resistance of the CoNiCrFeMn high entropy alloy under extreme irradiation flux [J]. *Nanotechnology*, 2020, 31(2): 025703.
- [5] LU Xiao-chong, ZHAO Jian-feng, YU Chao, LI Zhi-ming, KAN Qian-hua, KANG Guo-zheng, ZHANG Xu. Cyclic plasticity of an interstitial high-entropy alloy: Experiments, crystal plasticity modeling, and simulations [J]. *Journal of the Mechanics and Physics of Solids*, 2020, 142: 103971.
- [6] QIU Ji, JIN Tao, XIAO Ge-sheng, WANG Zai, LIU Er-qiang, SU Bu-yun, ZHAO Dan, SHU Xue-feng. Effects of pre-compression on the hardness of CoCrFeNiMn high entropy alloy based an asymmetrical yield criterion [J]. *Journal of Alloys and Compounds*, 2019, 802: 93–102.
- [7] WANG A G, AN Xiang-hai, GU Ji, WANG Xue-gang, LI Lin-lin, LI wei-lin, SONG Min, DUAN Qi-qiang, ZHANG Zhe-feng, LIAO Xiao-zhou. Effect of grain size on fatigue cracking at twin boundaries in a CoCrFeMnNi high-entropy alloy [J]. *Journal of Materials Science & Technology*, 2020, 39(4): 3–8.
- [8] YANG Li-xin, GE Hua-long, ZHANG Jian, XIONG Ting, JIN Qian-qian, ZHOU Yang-tao, SHAO Xiao-hong, ZHANG Bo, ZHU Zheng-wang, ZHENG Shi-jian, MA Xiu-liang. High He-ion irradiation resistance of CrMnFeCoNi high-entropy alloy revealed by comparison study with Ni and 304SS [J]. *Journal of Materials Science & Technology*, 2019, 35(3): 74–79.
- [9] GEORGE E P, CURTIN W A, TASAN C C. High entropy alloys: A focused review of mechanical properties and deformation mechanisms [J]. *Acta Materialia*, 2019, 188: 435–474.
- [10] LIU Wei-hong, WU Yuan, HE Jun-yang, NIEH T G, LU Zhao-ping. Grain growth and the Hall–Petch relationship in a high-entropy FeCrNiCoMn alloy [J]. *Scripta Materialia*, 2013, 68(7): 526–529.
- [11] SEOL J B, BAE J W, LI Zhi-ming, HAN Jong-chan, KIM J G, RAABE D, KIM H S. Boron doped ultrastrong and ductile high-entropy alloys [J]. *Acta Materialia*, 2018, 151: 366–376.
- [12] JIANG Jun, CHEN Peng-wan, QIU Jia-li, SUN Wei-fu, SAIKOV I, SHCHERBAKOV V, ALYMOV M. Microstructural evolution and mechanical properties of Al_xCoCrFeNi high-entropy alloys under uniaxial tension: A molecular dynamics simulations study [J]. *Materials Today Communications*, 2021, 28: 102525.
- [13] CAO Fu-hua, WANG Yun-jiang, DAI Lan-hong. Novel atomic-scale mechanism of incipient plasticity in a chemically complex CrCoNi medium-entropy alloy associated with inhomogeneity in local chemical environment [J]. *Acta Materialia*, 2020, 194: 283–294.
- [14] PANZARINO J F, PAN Z, RUPERT T J. Plasticity-induced restructuring of a nanocrystalline grain boundary network [J]. *Acta Materialia*, 2016, 120: 1–13.
- [15] PRAKASH A, WEYGAND D, BITZEK E. Influence of grain boundary structure and topology on the plastic deformation of nanocrystalline aluminum as studied by atomistic simulations [J]. *International Journal of Plasticity*, 2017, 97: 107–125.
- [16] PLIMPTON S. Fast parallel algorithms for short-range molecular dynamics [J]. *Journal of Computational Physics*, 1995, 117: 1–19.
- [17] FARKAS D, CARO A. Model interatomic potentials and lattice strain in a high-entropy alloy [J]. *Journal of Materials Research*, 2018, 33(19): 3218–3225.
- [18] STUKOWSKI A. Visualization and analysis of atomistic simulation data with OVITO–The open visualization tool [J]. *Modelling and Simulation in Materials Science and Engineering*, 2010, 18(1): 2154–2162.
- [19] STUKOWSKI A. Structure identification methods for atomistic simulations of crystalline materials [J]. *Modelling and Simulation in Materials Science and Engineering*, 2012, 20(4): 045021.
- [20] STUKOWSKI A, BULATOV V V, ARSENLIS A. Automated identification and indexing of dislocations in crystal interfaces [J]. *Modelling and Simulation in Materials Science and Engineering*, 2012, 20(8): 085007.
- [21] LIU Jun. Molecular dynamic study of temperature dependence of mechanical properties and plastic inception of CoCrCuFeNi high-entropy alloy [J]. *Physics Letters A*, 2020, 384(22): 126516.
- [22] ZHU Yun-tian, LIAO Xiao-zhou, WU Xiao-lei. Deformation twinning in nanocrystalline materials [J]. *Progress in Materials Science*, 2012, 57(1): 1–62.
- [23] LI Jia, FANG Qi-hong, LIAW P K, LIU Feng, LIU Yong. Effects of temperature and strain rate on plastic deformation mechanisms of nanocrystalline high-entropy alloys [J].

- Intermetallics, 2020, 120: 106741.
- [24] KIM Y K, LEE B J, HONG S K, HONG S L. Strengthening and fracture of deformation-processed dual fcc-phase CoCrFeCuNi and CoCrFeCu_{1.71}Ni high entropy alloys [J]. Materials Science and Engineering A, 2020, 781: 139241.
- [25] DUPRAZ M, SUN Z, BRANDL C, SWYGENHOVEN H V. Dislocation interactions at reduced strain rates in atomistic simulations of nanocrystalline Al [J]. Acta Materialia, 2018, 144: 68–79.
- [26] SWYGENHOVEN H V, WEERTMAN J R. Deformation in nanocrystalline metals [J]. Materials Today, 2006, 9: 24–31.
- [27] HALL E O. The deformation and ageing of mild steel: III Discussion of results [J]. Proceedings of the Physical Society Section B, 2002, 64(6): 495.
- [28] PETCH N J. The cleavage strength of polycrystals [J]. J Iron Steel Inst, 1953, 174: 25–28.
- [29] KNAPP J A, FOLLSTAEDT D M. Hall–Petch relationship in pulsed-laser deposited nickel films [J]. Journal of Materials Research, 2004, 19(1): 218–227.
- [30] CHEN Ji, LU Lin-qiong, LU Ke. Hardness and strain rate sensitivity of nanocrystalline Cu [J]. Scripta Materialia, 2006, 54(11): 1913–1918.
- [31] CHOKSHI A H, ROSEN A, KARCH J, GLEITER H. On the validity of the Hall–Petch relationship in nanocrystalline materials [J]. Scripta Metallurgica, 1989, 23: 1679–1683.
- [32] LU Ke, WEI Wen-duo, WANG Jing-tang. Microhardness and fracture properties of nanocrystalline Ni–P alloy [J]. Scripta Metallurgica et Materiala, 1990, 24(12): 2319–2323.
- [33] FEENSTRA B J, MAREL D, BARBER Z H, PINAYA R P, ERB U. Room temperature creep behavior of nanocrystalline nickel produced by an electrodeposition technique [J]. Materials Science and Engineering A, 1997, 237: 150–158.
- [34] HU Jian, SHI Y N, SAUVAGE X, SHA Gang, LU Ke. Grain boundary stability governs hardening and softening in extremely fine nanograined metals [J]. Science Foundation in China, 2017, 355(2): 1292.
- [35] CHEN Da. Structural modeling of nanocrystalline materials [J]. Computational Materials Science, 1995, 3(3): 327–333.

纳米 CoCrCuFeNi 高熵合金原子尺度的实时变形行为

全永刚¹, 田楠¹, 陈浩², 张显程², 胡永乐¹, 吉希希¹, 张明军¹, 赵超杰¹

1. 长沙理工大学 汽车与机械工程学院, 长沙 410114;

2. 华东理工大学 机械与动力工程学院, 上海 200237

摘要: 通过分子动力学方法分别在 $2 \times 10^8 \sim 1 \times 10^{10} \text{ s}^{-1}$ 的不同应变率和 10~1200 K 的不同温度下进行拉伸试验, 并研究纳米 CoCrCuFeNi 高熵合金的实时变形行为。结果表明, 在高温和低应变速率下的主要变形机制是晶界滑移。随着温度的降低和应变速率的增加, 位错滑移取代晶界滑移来控制塑性变形, 进而提高合金的强度。此外, 为进一步研究晶界对力学行为的影响, 对具有不同晶粒尺寸的合金进行模拟。结果发现, 当晶粒尺寸过小时, 纳米高熵合金的强度随着晶粒尺寸的增加而增加, 表现出反 Hall–Petch 关系。

关键词: 纳米高熵合金; 错位演化; 变形机制; 应变速率; 晶粒尺寸

(Edited by Bing YANG)